COMMUNICATIONS

NMR Determination of the Torsion Angle Ψ in α-Helical Peptides and Proteins: The HCCN Dipolar Correlation Experiment

Vladimir Ladizhansky, Mikhail Veshtort, and Robert G. Griffin[1]

Francis Bitter Magnet Laboratory and Department of Chemistry, Massachusetts Institute of Technology, Cambridge, Massachusetts 02139

Several existing methods permit measurement of the torsion angles ϕ, ψ and χ in peptides and proteins with solid-state MAS NMR experiments. Currently, however, there is not an approach that is applicable to measurement of ψ in the angular range $-20°$ to $-70°$, commonly found in α-helical structures. Accordingly, we have developed a HCCN dipolar correlation MAS experiment that is sensitive and accurate in this regime. An initial REDOR driven $^{13}C'-^{15}N$ dipolar evolution period is followed by the C' to C_α polarization transfer and by Lee–Goldburg cross polarization recoupling of the $^{13}C_\alpha{}^1H$ dipolar interaction. The difference between the effective $^{13}C^1H$ and $^{13}C^{15}N$ dipolar interaction strengths is balanced out by incrementing the $^{13}C-^{15}N$ dipolar evolution period in steps that are a factor of $R (R \sim \omega_{CH}/\omega_{CN})$ larger than the $^{13}C-^1H$ steps. The resulting dephasing curves are sensitive to variations in ψ in the angular region associated with α-helical secondary structure. To demonstrate the validity of the technique, we apply it to *N*-formyl-[U-^{13}C,^{15}N] Met-Leu-Phe-OH (MLF). The value of ψ extracted is consistent with the previous NMR measurements and close to that reported in diffraction studies for the methyl ester of MLF, *N*-formyl-[U-^{13}C,^{15}N]Met-Leu-Phe-OMe. © 2002 Elsevier Science (USA)

INTRODUCTION

Solid-state NMR (SSNMR) is emerging as an important tool for constraining molecular geometry, particularly in systems which cannot be studied with conventional approaches (*1*). Thus, significant information pertinent to the structure and function of biological solids is frequently obtained with a variety of SSNMR techniques (*2–6*). Recently, substantial efforts have been made to improve and broaden the range of applicability of SSNMR. Various techniques for homonuclear and heteronuclear distance measurements have been developed to constrain the secondary structure of peptides and proteins (*7–15*). In addition, a variety of experimental approaches which facilitate measurement of torsion angles in these systems have been published. In gen-

eral, torsion angle measurements are correlation experiments in which the mutual orientation of the anisotropic interactions such as chemical shift anisotropies and/or dipolar couplings is determined. If the orientations of these interactions with respect to the molecular frame are known, then correlation experiments can directly lead to important geometrical constraints. For example, one approach to determining the angle ψ involves correlating the orientation of the C' CSA tensor with that of the C_α–H dipolar coupling tensor (*16–18*). In this case, however, the data interpretation requires knowledge of the magnitude and orientation of the principal values of the chemical shift tensor (CSA) which are not known *a priori*, making data interpretation less than straightforward. In this respect, the choice of correlating the orientation of two dipolar interactions is easier since their orientations are well defined. This approach has been employed in several recent studies (*19–25*). For example, a significant deviation from the planar *trans*-conformation in the $^1H^{13}C-$ $^{13}C^1H$ molecular moieties of retinal in two membrane proteins bacteriorhodopsin and rhodopsin was detected by correlating the orientation of the two $^{13}C^1H$ dipolar tensors (*20, 26, 27*). In these experiments, the double quantum (DQ) coherence is first excited between two ^{13}C's and then allowed to evolve under the influence of the dipolar fields of the neighboring protons, resulting in measurement of the angle χ (*19*). Similar approaches are used in measurements of the torsion angle ϕ in the $^1H^{15}N-$ $^{13}C^1H$ spin quartet (*21, 28, 29*).

Another backbone torsion angle ψ can also be determined via dipolar correlation experiments. In this case the two dipole couplings that can be correlated are the $^{15}N^{13}C$ vectors in an $^{15}N^{13}C-^{13}C^{15}N$ moiety following excitation of the $^{13}C_\alpha-^{13}C'$ DQ coherence (*22, 23*). The $^{15}N-^{13}C$ interaction is restored by simultaneous phase inversion rotary resonance (SPI-R³) (*22*) or via a train of π-pulses applied to the ^{15}N channel (*23*). The resulting dephasing curves are sensitive to the variation of the ψ torsion angle in the neighborhood of *trans*-conformation $\pm(120°-180°)$ corresponding to a β-sheet regime.

In contrast to the situation found for β-sheets, the NCCN moiety in α-helical conformations is far from being planar, with

---

[1] To whom correspondence should be addressed. E-mail: rgg@mit.edu or griffin@ccnmr.mit.edu.

Ⓐ𝒫

the ψ values ranging between $-20°$ and $-70°$. Therefore, the $^{15}N^{13}C-^{13}C^{15}N$ experiment is outside its region of optimal sensitivity. To address this problem, we have developed a new experiment which correlates $^1H^{13}C_\alpha$ and $^{13}C'^{15}N$ dipolar interactions in the $^1H^{13}C_\alpha-^{13}C'^{15}N$ spin quartet. In the α-helical regime the $\theta_{N-C'-C_\alpha-H}$ dihedral angle lies in the vicinity of *trans*-conformation, and the NMR response is sensitive to variations in the $\theta_{N-C'-C_\alpha-H}$. The approach correlates strong interactions between directly bonded nuclear spins and can be used for multiple angle determination in uniformly labeled compounds. The utility of the experiment is demonstrated with investigations of N-formyl[U-$^{13}C,^{15}N$]Met-Leu-Phe-OH.

EXPERIMENTAL

NMR experiments were performed using an electronics console custom designed by Cambridge Instruments (courtesy of D. J. Ruben) that is mated with a Magnex Scientific (Abington, England) 11.7 T/104-mm-bore magnet (500.06 MHz for ^1H, 125.7 MHz for ^{13}C, and 50.6 MHz for ^{15}N, respectively). The triple resonance 4-mm Chemagnetics/Varian (Fort Collins, CO) MAS probe was used in the experiments and the spinning frequency, $\omega_r/2\pi = 12.9$ kHz, was controlled by Doty Scientific (Columbia, SC) spinning frequency controller to a stability of ±3 Hz.

The experiments were performed using the pulse sequence depicted in Fig. 1a. The selective excitation in the sequence was achieved by applying a modified SELDOM (*30*) pulse train, $[delay-(\pi/2)_x-zfilter-(\pi/2)_{\bar{y}}]_n$, where the carrier frequency was placed at C_α resonance. During the delay, C' magnetization makes $90°$ rotation in the xy-plane and is then restored to the z-axis by a hard $\pi/2$ pulse. The C_α magnetization remaining in the xy-plane is destroyed during the z-filter period, while the final $\pi/2$ pulse restores the z-magnetization to the xy-plane. A value of $n = 2$ was sufficient to saturate C_α while preserving $\sim90\%$ of C' magnetization. An 86-kHz TPPM decoupling (*31*) with overall phase shift of $15°$ was employed during acquisition. An ^1H RF field of ~65 kHz was applied during the Lee–Goldburg cross polarization (LGCP) (*32*) with the resulting effective field of $\omega_{eff} \sim 80$ kHz. To implement LGCP we used a theoretically calculated offset value $\Delta\omega = \omega_{eff} \cos\theta_M$ for a desired ^1H effective field, where $\theta_M = 54.7°$. For the exact Lee–Goldburg (*33*) condition, the C–H dipolar coupling is scaled by a factor $k_{LGCP} = \sin\theta_M$. In practice, the LGCP dephasing curve for C_α was measured, and the true scaling factor, $T_{1\rho}$, and the Lorentzian apodization factor were extracted from the data and used in the simulations. The carbon field during LGCP was matched to the $n = 1$ Hartmann–Hahn condition, $\omega_{eff} - \omega_{1C} = \omega_r$.

To minimize signal losses during REDOR recoupling, the ^{15}N and the ^1H RF fields were mismatched by a factor >3 (*34, 35*). Specifically, during REDOR, we employed ~32 and ~115 kHz of CW RF on the ^{15}N and ^1H channels during pulses, respectively, and ~100 kHz TPPM decoupling with overall phase shift
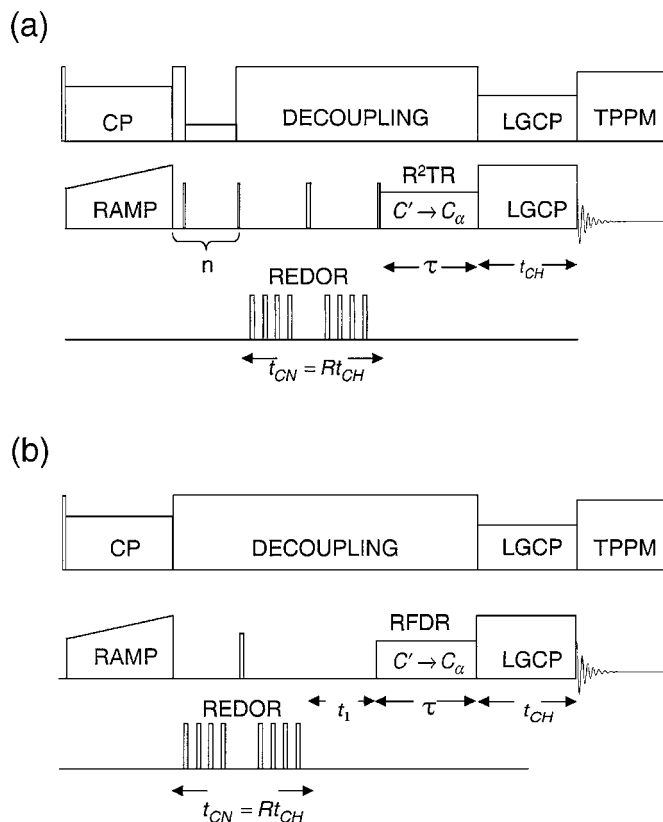

FIG. 1. (a) The 2D and (b) 3D pulse sequences for HCCN dipolar correlation experiments designed to measure the torsion angle ψ in α-helical peptides. In (a) ^{13}C polarization is generated with a ramp CP and a SELDOM filter suppresses the C_α magnetization leaving C' magnetization. During the REDOR and the LGCP periods the $^{13}C-^{15}N$ and $^{13}C-^1H$ dipole couplings evolve (for periods $t_{CN} = Rt_{CH}$, and t_{CH}, respectively). Following the REDOR period the C' polarization is transferred to C_α by R2TR. Finally the $^{13}C^1H$ dipole interaction is reintroduced with Lee–Goldburg cross polarization, and the signal is observed in the presence of TPPM decoupling. (b) The 3D experiment follows a similar approach except that an additional evolution period is introduced to yield a $^{13}C-^{13}C$ spectrum where the intensities in the third dimension are modulated by the dipolar coupling.

of $12°$ was employed during the free precession periods between the pulses (*13*). The finite (~16 μs) ^{15}N pulse lengths during REDOR led to an additional scaling of the $^{13}C/^{15}N$ dipolar coupling that must be incorporated into the analysis of the torsion angle data (*36*). In practice, the scaling factor was measured directly from a REDOR dephasing curve of C' resonance.

Following the REDOR recoupling is a period where selective polarization transfer occurs between the C' and C_α. This is accomplished with zero-quantum rotational resonance in the tilted frame (ZQ R^{2}TR) (*37, 38*), with the carrier frequency placed at the C_α resonance position. Application of a weak CW RF field ($\omega_1 \sim 2.2$ kHz) and a C' offset ($\Delta\omega_{C'} = 14.98$ kHz) was used to satisfy the ZQ resonance condition: $\sqrt{\omega_1^2 + \Delta\omega_{C'}^2} - \omega_1 = \omega_r$. Under these conditions the effective field for C_α resonance points
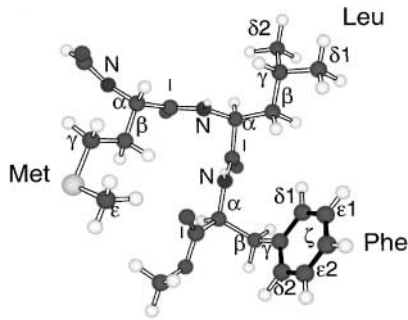
FIG. 2. The structure of N-formyl-L-Met-L-Leu-L-Phe-OMe as determined by X-ray crystallography (40).

along the rotating frame x-axis, whereas the effective field for C' is tilted by $\sim 8°$ from the z-axis. Under these circumstances we obtain a scaling factor $k_{R2TR} = -\frac{1}{8}(1 + \cos\beta_{C_\alpha}\cos\beta_{C'} + 2\sin\beta_{C_\alpha}\sin\beta_{C'}) \approx 0.09$, where $\beta_x = \arctan(\omega_1/\Delta\omega_x)$ (37, 38).

Another general version of the ψ torsion angle experiment more suitable for the multiple angle measurements is represented in Fig. 1b. Following the REDOR dephasing period, the C' resonances evolve according to their isotropic chemical shifts. Broadband dipolar recoupling (RFDR (35), SPC5 (11)) transfers polarization to the C_α spins, which is then dephased under LGCP. The dephasing of the (C', C_α) cross peaks in the 2D correlation spectrum as a function of dipolar evolution would be sensitive to the variation of ψ.

N-Formyl-[U-^{13}C,^{15}N]Met-Leu-Phe-OH (MLF) was prepared as described previously (39). Although the MLF crystal structure is not known, the structure of the methyl ester N-formyl-[U-^{13}C,^{15}N]Met-Leu-Phe-OMe is known (see Fig. 2) and the dihedral angle $\theta_{N_F-C'_L-C_{L\alpha}-H}$ equal to $-165.8°$ in MLF-OMe (40) is anticipated to be in the sensitive region of the HCCN experiment. We therefore chose this compound to demonstrate the technique.

THEORY AND SIMULATIONS

In the following discussion we use the symbols $C_{x,y,z}$, $N_{x,y,z}$, and $H_{x,y,z}$ to denote ^{13}C, ^{15}N, and ^{1}H spin operators. The pulse sequence in Fig. 1a generates transverse ^{13}C magnetization after ramped ^{1}H/^{13}C cross polarization. This is followed by the SELDOM sequence which suppresses signals from ^{13}C$_\alpha$ and preserves those from ^{13}C$'$. This defines an initial density matrix for the experiment: $\rho(0) = C'_x$. The C'_x density matrix evolves under two ^{13}C/^{15}N heteronuclear dipolar couplings arising from the directly bonded ^{15}N$_{i+1}$ ($\sim$900 Hz) and the remote ^{15}N$_i$ ($\sim$225 Hz) on the same residue. These two ^{13}C$'$–^{15}N dipolar interactions are reintroduced by REDOR π-pulses applied to the ^{15}N channel, while the π-pulse in the middle of the REDOR sequence on the ^{13}C channel refocuses ^{13}C chemical shifts. The REDOR sequence defines the t_{CN} evolution time of the experiment. The effective Hamiltonian of a ^{13}C coupled to two ^{15}N

spins generated by the REDOR pulses is (8)

$$H_{\text{REDOR}} = 2\omega_d^{C'N_{i+1}} C'_z N_{i+1z} + 2\omega_d^{C'N_i} C'_z N_{iz}. \quad [1]$$

This Hamiltonian generates a well-known dephasing behavior (41–43)

$$\rho(t_{CN}) = C'_x \cos\left(\omega_d^{C'N_{i+1}} t_{CN}\right) \cos\left(\omega_d^{C'N_i} t_{CN}\right) + \cdots, \quad [2]$$

where all antiphase coherences are omitted.

The ^{13}C$'$ magnetization modulated by ^{13}C/^{15}N dipolar couplings is selectively transferred to the ^{13}C$_\alpha$ via ZQ R^{2}TR. The $90°$ pulse prior to R^{2}TR period aligns the C$'$ magnetization with the effective field. Since ZQ R^{2}TR polarization transfer process is anisotropic, the quantity of polarization transferred to C$_\alpha$ after time τ will be a function of the crystallite orientation. The ZQ R^{2}TR effective Hamiltonian (37, 38)

$$H_{\text{R}^2\text{TR}} = \omega_d^{CC}[C_\alpha^- C'^+ + C_\alpha^+ C'^-] \quad [3]$$

generates polarization transfer of the form

$$\rho(t_{CN}) = C_{\alpha x} \cos\left(\omega_d^{C'N_{i+1}} t_{CN}\right)$$
$$\times \cos\left(\omega_d^{C'N_i} t_{CN}\right) \sin^2\left(\omega_d^{CC}\tau\right) + \cdots, \quad [4]$$

where only terms corresponding to polarization of the C$_\alpha$ spin are kept.

The ^{13}C$_\alpha$–^{1}H dipolar interaction is then reintroduced through the LGCP, defining t_{CH}. As shown previously, the LGCP dynamics of a ^{13}C^{1}H group are nearly independent of spinning frequency at $\omega_r/2\pi \geq 13$ kHz and is dominated by the strong ^{13}C–^{1}H dipolar coupling (44). In a two spin approximation, the ZQ Hamiltonian generated by LGCP can be written as (32)

$$H_{\text{LGCP}} = \omega_d^{C_\alpha H}[C_\alpha^- H^+ + C_\alpha^+ H^-] \quad [5]$$

and part of the density matrix of the crystallite corresponding to the C$_{\alpha x}$ observable becomes

$$\rho(t_{CN}, t_{CH}) = \frac{1}{2} C_{\alpha x} \cos\left(\omega_d^{C'N_{i+1}} t_{CN}\right) \cos\left(\omega_d^{C'N_i} t_{CN}\right)$$
$$\times \sin^2\left(\omega_d^{CC}\tau\right)\left[1 + \cos\left(\omega_d^{C_\alpha H} t_{CH}\right)\right]. \quad [6]$$

The effective dipolar couplings $\omega_d^{C'N_j}$, ω_d^{CC}, and $\omega_d^{C_\alpha H}$ depend on the crystallite orientation and can be written as (32, 38, 45)

$$\omega_d^{C'N_j}\left(\Omega, \Omega_{PM}^{C'N_j}\right) = -\frac{4}{\pi} k_{\text{REDOR}} \text{Im}\left(\omega_{(1)}^{C'N_j}\right),$$
$$\omega_d^{CC}\left(\Omega, \Omega_{PM}^{CC}\right) = k_{\text{R}^2\text{TR}}\left|\omega_{(1)}^{CC}\right| \quad [7]$$
$$\omega_d^{C_\alpha H}\left(\Omega, \Omega_{PM}^{C_\alpha H}\right) = \frac{1}{4} k_{\text{LGCP}}\left|\omega_{(1)}^{C_\alpha H}\right|,$$

where

$$\omega_{(1)}^{AB} = \frac{\mu_0}{4\pi} \frac{\gamma_A \gamma_B \hbar^2}{r_{AB}^3} \sum_{m=-2}^{2} D_{0,m}^{(2)}(\Omega_{PM}^{AB}) D_{m,-1}^{(2)}(\Omega) d_{-1,0}^{(2)}(\theta_M) \quad [8]$$

and A and B denote different nuclei: C', N_j, H, C_α. The scaling factor k_{REDOR} in the expression for the $\omega_d^{C'N}$ effective $^{13}C/^{15}N$ dipolar coupling during the REDOR experiment is $\cos(\pi/2\varphi)/(1-\varphi^2)$, where φ is a fraction of the rotor period $\varphi = 2\tau_\pi/T_R$ occupied by pulses of length τ_π (36). The correction arises because the pulses occupy a significant fraction of the rotor period. The scaling factors k_{R2TR} and k_{LGCP} were defined earlier.

The Wigner rotation matrices $D_{0,m}^{(2)}(\Omega_{PM}^{C'N_j})$, $D_{0,m}^{(2)}(\Omega_{PM}^{C'N_\alpha})$, and $D_{0,m}^{(2)}(\Omega_{PM}^{C_\alpha H})$ describe transformations of the corresponding $C'N_j$, $C'C_\alpha$, and $C_\alpha N$ dipole tensors from their principal axis systems (PAS) to the molecular frame which can be conveniently chosen to coincide with the PAS of the $C'C_\alpha$ dipole tensor. The Euler angles $\Omega_{PM}^{C_\alpha H} = (0, \pi - \theta_{C'-C_\alpha-H}, \gamma_{C_\alpha H})$, $\Omega_{PM}^{C'N_1} = (0, \theta_{N_1-C'-C_\alpha}, \gamma_{C'N_1})$, $\Omega_{PM}^{C'N_2} = (0, \pi - \theta_{C'-C_\alpha-N_2}, \gamma_{C'N_2})$ determine the orientation of the principal axis systems with respect to the molecular frame, and the Euler angles Ω are random variables in a powder and relate the molecular frame to a rotor frame. The $H-C_\alpha-C'-N_{i+1}$ dihedral angle denoted by ζ in the following is equal to the difference in Euler angles $\gamma_{C'N_{i+1}} - \gamma_{C_\alpha H}$ and for L-amino acids can be approximately related to the ψ ($N_i-C_\alpha-C-N_{i+1}$) torsion angle by

$$\psi = \zeta + 120°. \quad [9]$$

Assuming that bond angles are known, the intensity of the spectral line corresponding to the C_α will be a function of ψ only and can be written as

$$\langle S_{\alpha x}\rangle(t_{CN}, t_{CH}, \psi) = \frac{1}{8\pi^2} \int d\Omega \sin^2 \Phi_{CC} \cos \Phi_{C'N_1}$$
$$\times \cos \Phi_{C'N_2}[1 + \cos \Phi_{CH}], \quad [10]$$

where we introduce the dynamic phases

$$\Phi_{CC} = \omega_d^{CC}\tau$$
$$\Phi_{C'N_j} = \omega_d^{C'N_j} t_{CN} \quad [11]$$
$$\Phi_{CH} = \omega_d^{C_\alpha H} t_{CH}.$$

To compensate for transverse relaxation effects during REDOR dephasing and $T_{1\rho}$ effects during LGCP, a reference experiment should be recorded without π-pulses on the ^{15}N channel and the resulting curve can be represented in a REDOR-like manner. Finally, to account for possible broadening effects due to residual $^1H-^1H$ couplings, RF inhomogeneity, and differential relaxation, the Lorentzian apodization of the LGCP dephasing

was used. This results in the final expression,

$$\frac{S_F}{S_0}(t_{CN}, t_{CH}, \psi)$$
$$= \frac{\int d\Omega \sin^2 \Phi_{CC}(\Omega) \cos \Phi_{C'N_{i+1}}(\Omega) \cos \Phi_{C'N_i}[1 + e^{-t_{CH}/T_2'} \cos \Phi_{CH}(\Omega, \psi)]}{\int d\Omega \sin^2 \Phi_{CC}(\Omega)[1 + e^{-t_{CH}/T_2'} \cos \Phi_{CH}(\Omega, \psi)]},$$
$$[12]$$

where T_2' has a value of 0.9 ms extracted from the observation of LGCP dephasing. The dependence of the signal on ψ is the strongest if the phases $\Phi_{C'N_{i+1}}$ and Φ_{CH} are of the same order of magnitude. One can therefore increment t_{CN} and t_{CH} simultaneously, keeping the ratio between the increments approximately inversely proportional to the ratio of the corresponding interaction strengths: $R = t_{CN}/t_{CH} \approx \omega_d^{C_\alpha H}/\omega_d^{C'N_{i+1}}$. Here, it is necessary to account for the fact that $\omega_d^{C_\alpha H}$ and $\omega_d^{C'N_{i+1}}$ dipolar couplings have different angular dependence: $\omega_d^{C_\alpha H}$ is γ-encoded, i.e., depends solely on β, whereas $\omega_d^{C'N_{i+1}}$ depends on both β and γ. This makes an optimal R factor of the order of 14–18.

Figure 3a shows the backbone geometry with indicated ψ angle and Fig. 3b presents calculated dephasing curves based on the geometry of Fig. 3a, the experimentally determined scaling factors $k_{REDOR} = 0.92$, $k_{LGCP} = 0.82$, and with $|\zeta|$ varying from $130°$ to $180°$ in $10°$ steps. The calculations are performed
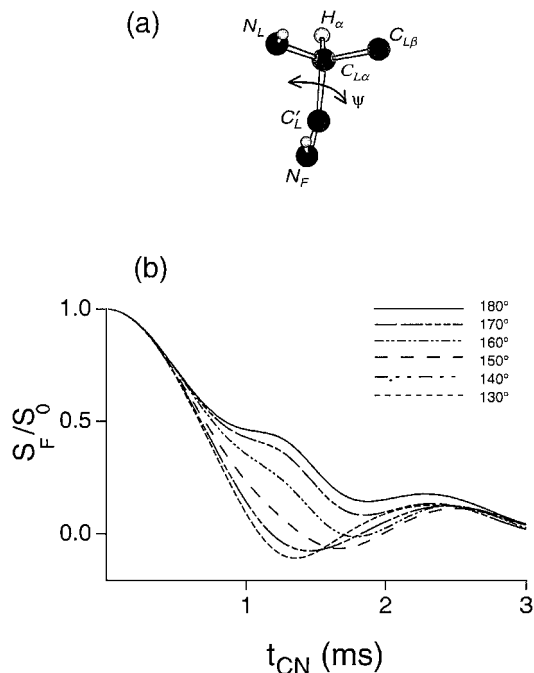

FIG. 3. (a) The relevant $H_\alpha-C_{L\alpha}-C_L'-N_F$ fragment of the MLF backbone geometry indicating the torsion angle ψ determined in the experiment. (b) Simulations of the HCCN dephasing curves as a function of the H–C–C–N dihedral angle. The following structural parameters were used in the simulations: $\theta_{N_F-C_L'-C_{L\alpha}} = 115.7°$, $\theta_{C_L'-C_{L\alpha}-H_\alpha} = 107.3°$, $\theta_{C_L'-C_{L\alpha}-N_L} = 110.2°$, $d_{N_F C_L'} = 1.338$ Å, $d_{C_{L\alpha} C_L'} = 1.533$ Å, $d_{C_{L:\alpha} H} = 1.115$ Å, $d_{C_{L\alpha} N_L} = 1.462$ Å.

by numerical integration of Eq. [12] for the scaling factor $R = 16$.

Like other torsion angle experiments using dipole–dipole correlations, the HCCN experiment has reflection symmetry with respect to the *trans*-plane and the result is insensitive to the sign of ζ. Therefore, the experiment provides two values for ζ and similarly for ψ. This ambiguity can be eliminated for most amino acids by comparing the ψ values with a Ramachandran plot. The allowed ψ for the α-helical conformation is confined to the region from $-20°$ to $-70°$, corresponding to ζ values ranging from $-140°$ to $-190°$ as shown in Fig. 4.

The center of mirror symmetry ($\zeta = \pm 180°$) is therefore shifted toward the edge of the most populated conformational region. The conformations with ζ beyond that region are much less likely to occur. However, some ambiguity is possible if the measured dihedral angle ζ falls in the region $-180° \pm 10°$. In this case the two possible solutions for ζ will lead to ψ values which are both allowed. Additional information is then required to constrain ψ without ambiguity.

The most sensitive region of this experiment is in the range of $|\zeta| \sim 150°$–$170°$, whereas values of $|\zeta| < 120°$ are difficult to distinguish from one another. In addition, the dependence of the dephasing on $|\zeta|$ exhibits a singularity around $80°$ with the corresponding curve resembling the one for $145°$. However, since the values of $\zeta > -140°$ are much less likely to occur, this ambiguity can be eliminated in many cases and solutions lying outside the Ramachandran plot can be discarded.

There are a few sources of systematic error encountered in extracting ψ from the experimental data. One is determined by approximating LGCP by the time-independent Hamiltonian of Eq. [5]. At high spinning frequencies the full LGCP Hamiltonian is dominated by the time-independent part which is a sum of spin pair terms of the type of Eq. [5]:

$$H_{\text{LGCP}} = \omega_d^{C_\alpha H}[C_\alpha^- H_\alpha^+ + C_\alpha^+ H_\alpha^-]$$
$$+ \sum_{i,j \neq \alpha} \omega_d^{C_i H_j}[C_i^- H_j^+ + C_i^+ H_j^-]. \qquad [13]$$
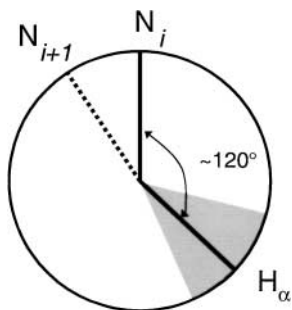
FIG. 4. Illustration of the relation between the ζ (H–C–C–N) dihedral angle determined in the experiment and ψ torsion angle. The ζ angle directly measured here is related to ψ by $\psi \approx \zeta + 120°$. Both angles are negative as drawn here. The shadowed region corresponds to α-helical geometry for ζ.
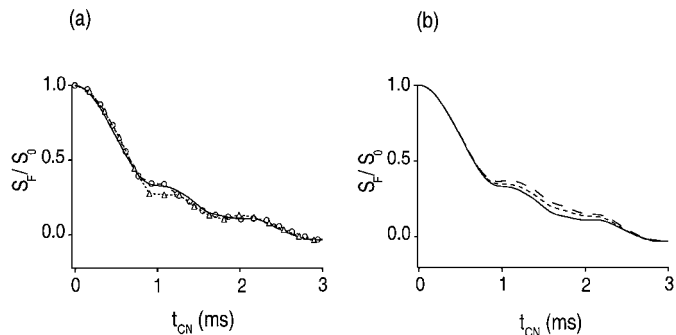
FIG. 5. (a) A comparison between the dephasing curves obtained from the analytical expression of Eq. [12] (solid line), and exact calculation in the N_2–C–C–H spin systems for $\omega_r/2\pi = 12.9$ kHz (circles). The calculation was performed assuming ideal pulses and no relaxation. For comparison, a full simulation for $\omega_r/2\pi = 11$ kHz (triangles) is shown. (b) Illustration of the effects of variations of the geometrical input parameters on the dephasing curves: (solid line) analytical curve for $\theta_{C'-C_\alpha-H} = 107.3°$, $\zeta = -165.8°$; (short-dashed line) curve corresponding to a $5°$ deviation of the $\theta_{C'-C_\alpha-H}$ bond angle. For comparison, the long-dashed line shows a curve corresponding to $+5°$ deviation of ζ. The $-5°$ deviation of the $\theta_{C'-C_\alpha-H}$ results in faster HCCN dephasing which is smaller than the curve for $-5°$ deviation of ζ.

In general the various terms in Eq. [13] do not commute, which affects the spin dynamics (*44, 46*). These effects are independent of the spinning frequency. The other two contributions are the residual ^{1}H–^{1}H dipolar couplings which are generally small, since H_α is usually isolated from the rest of the proton bath and the dipolar interactions are significantly reduced by the Lee–Goldburg decoupling (*33*), and time-dependent ^{1}H–^{13}C dipolar terms neglected in Eq. [13], which are an explicit function of ω_r. To estimate the relative role of these effects, an exact multispin calculation was performed for N_2CCH_3 and N_2CCH spin systems and compared with the numerically integrated analytical expression of Eq. [12]. All simulations were done assuming the geometry of MLF-OMe ($\zeta = -165.8°$), and $T_2' = \infty$. Figure 5a compares exact simulation of the NMR response of the N_2CCH spin system with the analytical expression, and there is rather good agreement between two simulations. Increasing the number of ^{1}H's has a negligible effect on the dephasing curves and the result of the exact simulation in the $N_2CC–H_3$ spin system is the same. For comparison, a simulation for $\omega_r/2\pi = 11$ kHz is also shown. In this case the deviation from the "ideal" behavior of Eq. [12] is more pronounced, but overall the error introduced by the time independent approximation of Eq. [5] remains tolerable.

Additional significant contributions to the systematic error of the experiment arise from the uncertainty in the geometric parameters required for data interpretation. One is related to some uncertainty of the bond angles. This issue is explored in Fig. 5b, where the analytical dephasing curve from Fig. 5a ($\theta_{C'-C_\alpha-H} = 107.3°$, $\zeta = -165.8°$) is duplicated and plotted together with the curve corresponding to $\theta_{C'-C_\alpha-H} = 112.3°$, $\zeta = -165.8°$. The deviation is obvious but still within $5°$. For comparison, a curve for $\theta_{C'-C_\alpha-H} = 107.3°$, $\zeta = -170.8°$ is
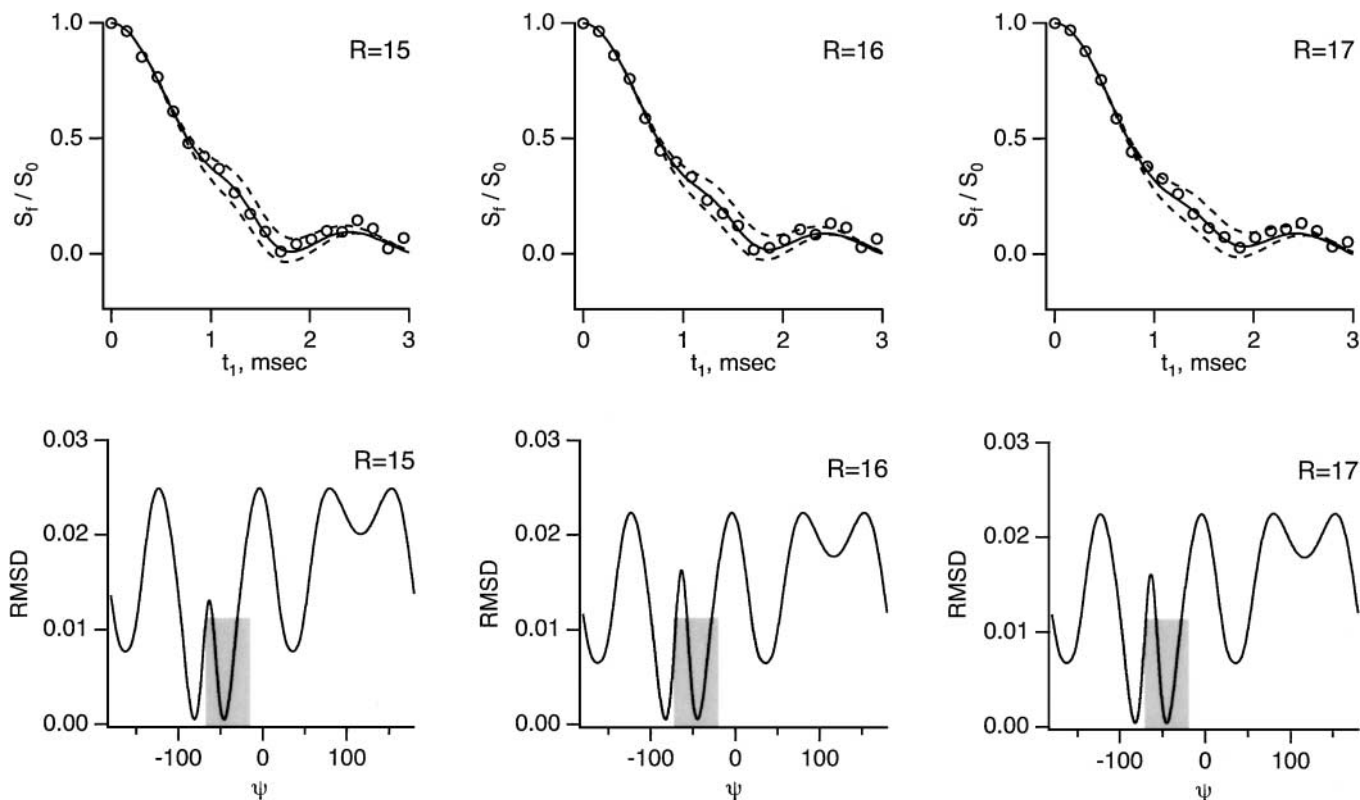
FIG. 6. (a)–(c) Experimental results of NCCH measurement of the H_α–$C_{L\alpha}$–C'_L–N_F dihedral angle. The measurements were done for three different R values as indicated in the figures. The dashed lines correspond to the $\pm 5°$ deviation from the best fit. (d)–(f) RMSD plots of the experiments for R values as indicated in the figures. The shadowed sections on the RMSD plots show regions corresponding to the allowed α-helical conformations.

also shown. Thus, like the other torsion angle experiments the HCCN experiment is sensitive to the variation of the bond angles. However, the total uncertainty of these parameters would not result in an error larger than $5°$ in the ψ value.

Another uncertainty arises when the relation $\psi = \zeta + 120°$, which is based on the assumption of perfect tetrahedral geometry, is used. In fact, deviations from tetrahedral structure are well known and should be taken incorporated into estimates of the accuracy of the experiment, which is a general problem inherent to most torsion angle experiments. We can estimate therefore that the systematic error introduced by uncertainty in structural input parameters generally exceeds that resulting from modeling spin dynamics by the time-independent Hamiltonians.

RESULTS AND DISCUSSION

The experimental test of the HCCN torsion angle experiment was performed on MLF-OH. The X-ray structure of the closely related MLF-OMe provides a value for the $\theta_{N_F-C'_L-C_{L\alpha}-H}$ dihedral angle of $-165.8°$. Although these two forms may differ, other NMR measurements (*13, 29*) suggest that the difference is not very significant. To translate the $\theta_{N_F-C'_L-C_{L\alpha}-H}$ into ψ, we used the relation

$$\psi = \theta_{N_F-C'_L-C_{L\alpha}-H} + 116.5°$$

which is strictly valid only for MLF-OMe.

Figures 6a–6c display the experimental dephasing curves for the $R = 15$, 16, and 17, respectively, and Figs. 6d–6f show the corresponding RMSD plots. The data showing the best fits are summarized in Table 1. The simulated dephasing curves are plotted on the same graphs together with the curves differing from the best fit by $\pm 5°$, which represents a conservative estimate of the experimental accuracy. The deviation of the experimental curves from those predicted for $t_{CN} > 2$ ms is partially due to the low signal-to-noise ratio, since most of the signal had dephased.

TABLE 1
ψ Torsion Angle Values Extracted from the Experiments with Different R

R	$\partial_{H-C_{L\alpha}-C'_L-N_F}$	ψ
15	$\pm 162.5°$	-46, 82.2
16	$\pm 161.1°$	$-44.6°$, 80.8°
17	± 161.9	$-45.4°$, 81.6°

In larger peptides and proteins, where signal-to-noise ratio is lower than in model compounds, one can use a *J*-decoupled version of REDOR (*47*) which would partially reduce a signal loss due to homonuclear *J*-couplings. Some deviations are also expected due to factors discussed in the previous section.

The small discrepancy between experiments for different values of *R* is well within the expected error margin. The dashed regions on the RMSD plots in Figs. 4d–4f indicate the α-helical region-($20°–70°$). One solution is clearly well outside the region and we can conclude that the dephasing curves correspond to the $\psi = -45° \pm 5°$.

CONCLUSIONS

We have demonstrated a new method for measuring the torsion angle Ψ in peptides and proteins which is applicable to systems containing the α-helical motif. The results indicate that the HCCN experiment is a feasible method for an accurate determination of the ψ angle in this regime of the Ramachandran plot where other methods do not provide accurate results. The experiment can be applied to uniformly ^{13}C/^{15}N-labeled compounds and benefits from high spinning frequencies. At spinning frequencies >12 kHz, we obtain a simple mathematical expression for the signal which facilitates analysis of the experimental data.

ACKNOWLEDGMENTS

REFERENCES

1. R. G. Griffin, Dipolar recoupling in MAS spectra of biological solids, *Nature Struct. Biol.* **5,** 508–512 (1998).

2. F. Creuzet, A. Mcdermott, R. Gebhard, K. V. D. Hoef, M. B. Spijker-Assink, J. Herzfeld, J. Lugtenburg, M. H. Levitt, and R. G. Griffin, Determination of membrane protein structure by rotational resonance NMR: Bacteriorhodopsin, *Science* **251,** 783–786 (1991).

3. K. V. Lakshmi, M. Auger, J. Raap, J. Lutenburg, R. G. Griffin, and J. Herzfeld, Internuclear distance measurement in a reaction intermediate: Solid-state ^{13}C NMR rotational resonance determination of the Schiff-base configuration in the M-photointermediate of bacteriorhodopsin, *J. Am. Chem. Soc.* **115,** 8515–8516 (1993).

4. P. T. Lansbury, P. R. Costa, J. M. Griffiths, E. J. Simon, M. Auger, K. J. Halverson, D. A. Kocisko, Z. S. Hendsch, T. T. Ashburn, R. G. S. Spencer, B. Tidor, and R. G. Griffin, Structural model for the β-amyloid fibril based on interstrand alignment of an antiparallel-sheet comprising a C-terminal peptide, *Nature Struct. Biol.* **2,** 990–998 (1995).

5. J. J. Balbach, Y. Ishii, O. N. Antzutkin, R. D. Leapman, N. W. Rizzo, F. Dyda, J. Reed, and R. Tycko, Amyloid fibril formation by A(beta16–22), a seven residue fragment of the Alzheimer's beta-amyloid peptide, and structural characterization by solid state NMR, *Biochemistry* **39,** 13748–13759 (2000).

6. Alia, J. Matysik, C. Soede-Huijbregts, M. Baldus, J. Raap, J. Lugtenburg, P. Gast, H. J. V. Gorkom, A. J. Hoff, and H. J. M. de Groot, Ultrahigh field MAS NMR dipolar correlation spectroscopy of the histidine residues in light-harvesting complex II from photosynthetic bacteria reveals partial internal charge transfer in the B850/His complex, *J. Am. Chem. Soc.* **123,** 4803–4809 (2001).

7. D. P. Raleigh, M. H. Levitt, and R. G. Griffin, Rotational resonance in solid state NMR, *Chem. Phys. Lett.* **146,** 71–76 (1988).

8. T. Gullion and J. Schaefer, Rotational-echo double-resonance NMR, *J. Magn. Reson.* **81,** 196–200 (1989).

9. A. E. Bennett, D. P. Weliky, and R. Tycko, Quantitative conformational measurements in solid state NMR by constant-time homonuclear dipolar recoupling, *J. Am. Chem. Soc.* **120,** 4897–4898 (1998).

10. P. R. Costa, B. Sun, and R. G. Griffin, Rotational resonance tickling: Accurate internuclear distance measurement in solids, *J. Am. Chem. Soc.* **119,** 10821–10836 (1997).

11. M. Hohwy, H. J. Jakobsen, M. Edén, M. H. Levitt, and N. C. Nielsen, Broadband dipolar recoupling in the nuclear magnetic resonance of rotating solids: A compensated C7 pulse sequence, *J. Chem. Phys.* **108,** 2686–2694 (1998).

12. M. Hohwy, C. M. Rienstra, C. P. Jaroniec, and R. G. Griffin, Fivefold symmetric homonuclear dipolar recoupling in rotating solids: Application to double quantum spectroscopy, *J. Chem. Phys.* **110,** 7983–7992 (1999).

13. C. P. Jaroniec, B. A. Tounge, J. Herzfeld, and R. G. Griffin, Frequency selective heteronuclear dipolar recoupling in rotating solids: Accurate ^{13}C–^{15}N distance measurements in uniformly-^{13}C, ^{15}N-labeled peptides, *J. Am. Chem. Soc.* **123,** 3507–3519 (2000).

14. I. Sack, Y. S. Balazs, S. Rahimipour, and S. Vega, Solid-state NMR determination of peptide torsion angles: Applications of ^{2}H-dephased REDOR, *J. Am. Chem. Soc.* **122,** 12263–12269 (2000).

15. I. Sack, Y. S. Balazs, S. Rahimipour, and S. Vega, Peptide torsion angle measurements: Effects of nondilute spin pairs on carbon-observed, deuterium-dephased PM5-REDOR, *J. Magn. Reson.* **148,** 104–114 (2001).

16. K. Schmidt-Rohr, Torsion angle determination in solid ^{13}C-labeled amino acids and peptides by separated-local-field double-quantum NMR, *J. Am. Chem. Soc.* **118,** 7601–7603 (1996).

17. Y. Ishii, T. Terao, and M. Kainosho, Relayed anisotropy correlation NMR: Determination of dihedral angles in solids, *Chem. Phys. Lett.* **256,** 133–140 (1996).

18. T. Fujiwara, T. Shimomura, and H. Akutsu, Multidimensional solid-state nuclear magnetic resonance for correlating anisotropic interactions under magic-angle spinning conditions. *J. Magn. Reson.* **124,** 147–153 (1997).

19. X. Feng, Y. K. Lee, D. Sandström, M. Edén, H. Maisel, A. Sebald, and M. H. Levitt, Direct determination of a molecular torsional angle by solid-state NMR, *Chem. Phys. Lett.* **257,** 314–320 (1996).

20. X. Feng, P. J. E. Verdegem, Y. K. Lee, D. Sandström, M. Edén, P. Bovee-Geurts, W. J. De Grip, J. Lugtenburg, H. J. M. de Groot, and M. H. Levitt, Direct determination of a molecular torsional angle in the membrane protein rhodopsin by solid-state NMR, *J. Am. Chem. Soc.* **119,** 6853–6857 (1997).

21. M. Hong, J. D. Gross, and R. G. Griffin, Site-resolved determination of peptide torsion angle ϕ from the relative orientations of backbone N-H and C-H bonds by solid-state NMR, *J. Phys. Chem. B* **101,** 5869–5874 (1997).

22. P. R. Costa, J. D. Gross, M. Hong, and R. G. Griffin, Solid-state NMR measurement of ψ in peptides: A NCCN 2Q-heteronuclear local field experiment, *Chem. Phys. Lett.* **280,** 95–103 (1997).

23. X. Feng, M. Eden, A. Brinkmann, H. Luthman, L. Eriksson, A. Gräslund, O. N. Antzutkin, and M. H. Levitt, Direct determination of a peptide torsional angle ψ by double-quantum solid-state NMR, *J. Am. Chem. Soc.* **119,** 12006–12007 (1997).

24. B. Reif, M. Hohwy, C. P. Jaroniec, C. M. Rienstra, and R. G. Griffin, NH-NH vector correlation in peptides by solid state NMR, *J. Magn. Reson.* **145,** 132–141 (2000).

25. X. Feng, P. J. E. Verdegem, M. Edén, D. Sandström, Y. K. Lee, P. H. M. Boveegeurts, W. J. D. Grip, J. Lugtenburg, H. J. M. de Groot, and M. H. Levitt, Determination of a molecular torsional angle in the metarhodopsin-I photointermediate of rhodopsin by double-quantum solid-state NMR, *J. Biomol. NMR* **16,** 1–8 (2000).

26. J. C. Lansing, M. Hohwy, C. P. Jaroniec, A. F. L. Creemers, J. Lugtenburg, J. Herzfeld, and R. G. Griffin, Evolution of chromophore distortions in the bacteriorhodopsin photocycle determined by solid-state NMR, *Biophys. J.* **80,** 2728 (2001).

27. J. C. Lansing, M. Hohwy, C. P. Jaroniec, A. F. L. Creemers, J. Lugtenburg, J. Herzfeld, and R. G. Griffin, Determination of torsion angles in membrane proteins, submitted.

28. C. M. Rienstra, M. Hohway, L. J. Mueller, C. P. Jaroniec, B. Reif, and R. G. Griffin, Determination of multiple torsion angle constraints in U-^{13}C, ^{15}N-labeled peptides: 3D ^{1}H-^{15}N-^{13}C-^{1}H dipolar chemical shift spectroscopy in rotating solids, submitted.

29. C. M. Rienstra, M. Hohwy, L. J. Mueller, C. P. Jaroniec, B. Reif, and R. G. Griffin, 3D ^{1}H-^{13}C-^{13}C-^{1}H dipolar chemical shift spectroscopy in solids: Multiple torsion constraints in U-^{13}C, ^{15}N-labeled peptides, submitted.

30. P. Tekely, J. Brondeau, K. Elbayed, A. Retournard, and D. Canet, A simple pulse train, using 90° hard pulses, for selective excitation in high resolution solid state NMR, *J. Magn. Reson.* **80,** 509–516 (1988).

31. A. E. Bennett, C. M. Rienstra, M. Auger, K. V. Lakshmi, and R. G. Griffin, Heteronuclear decoupling in rotating solids, *J. Chem. Phys.* **103,** 6951–6957 (1995).

32. B.-J. van Rossum, C. P. de Groot, V. Ladizhansky, S. Vega, and H. J. M. de Groot, A method for measuring heteronuclear (^{1}H-^{13}C) distances in high speed MAS NMR, *J. Am. Chem. Soc.* **122,** 3465–3472 (2000).

33. M. Lee and W. I. Goldburg, Nuclear-magnetic-resonance narrowing by a rotating rf field, *Phys. Rev. A* **140,** 1261–1271 (1965).

34. Y. Ishii, J. Ashida, and T. Terao, ^{13}C-^{1}H dipolar recoupling dynamics in ^{13}C multiple-pulse solid-state NMR, *Chem. Phys. Lett.* **246,** 439–445 (1995).

35. A. E. Bennett, C. M. Rienstra, J. M. Griffiths, W. Zhen, P. T. Lansbury, and R. G. Griffin, Homonuclear radio frequency-driven recoupling in rotating solids, *J. Chem. Phys.* **108,** 9463–9479 (1998).

36. C. P. Jaroniec, B. A. Tounge, C. M. Rienstra, J. Herzfeld, and R. G. Griffin, Recoupling of heteronuclear dipolar interactions with rotational-echo double-resonance at high magic-angle spinning frequencies, *J. Magn. Reson.* **146,** 132–139 (2000).

37. K. Takegoshi, K. Nomura, and T. Terao, Rotational resonance in the tilted rotating frame, *Chem. Phys. Lett.* **232,** 424–428 (1995).

38. K. Takegoshi, K. Nomura, and T. Terao, Selective homonuclear polarization transfer in the tilted rotating frame under magic angle spinning in solids, *J. Magn. Reson.* **127,** 206–216 (1997).

39. C. M. Rienstra, M. Hohwy, M. Hong, and R. G. Griffin, 2D and 3D ^{15}N-^{13}C-^{13}C NMR chemical shift correlation spectroscopy of solids: Assignment of MAS spectra of peptides, *J. Am. Chem. Soc.* **122,** 10979–10990 (2000).

40. E. Gavuzzo, F. Mazza, G. Pochetti, and A. Scatturin, Crystal structure, conformation, and potential energy calculations of the chemotactic peptide N-formyl-L-Met-L-Leu-L-Phe-OMe, *Int. J. Peptide Protein Res.* **34,** 409–415 (1989).

41. C. A. Fyfe and A. R. Lewis, Investigation of the viability of solid-state NMR distance determinations in multiple spin systems of unknown structure, *J. Phys. Chem. B* **104,** 48–55 (2000).

42. K. Nishimura, A. Naito, S. Tuzi, and H. Saito, Analysis of dipolar dephasing pattern in I-S$_n$ multispin system for obtaining the information of molecular packing and its application to crystalline N-acetyl-Pro-Gly-Phe by REDOR solid state NMR, *J. Phys. Chem. B* **103,** 8398–8404 (1999).

43. J. M. Goetz and J. Schaefer, REDOR dephasing by multiple spins in the presence of molecular motion, *J. Magn. Reson.* **127,** 147–154 (1997).

44. V. Ladizhansky and S. Vega, Polarization transfer dynamics in Lee–Goldburg cross polarization nuclear magnetic resonance experiments on rotating solids, *J. Chem. Phys.* **112,** 7158–7166 (2000).

45. M. Mehring, "Principles of High Resolution NMR in Solids," Springer-Verlag, Berlin (1983).

46. E. Vinogradov, V. Ladizhansky, B.-J. van Rossum, H. J. M. de Groot, and S. Vega, Spin dynamics in heteronuclear uniformly labelled multi-spin systems under Lee Goldburg Cross Polarization conditions, in preparation.

47. C. P. Jaroniec, B. A. Tounge, C. M. Rienstra, J. Herzfeld, and R. G. Griffin, Measurement of ^{13}C-^{15}N distances in uniformly ^{13}C labeled biomolecules: J-decoupled REDOR, *J. Am. Chem. Soc.* **121,** 10237–10238 (1999).